Endotoxin Uptake by S1 Proximal Tubular Segment Causes Oxidative Stress in the Downstream S2 Segment

Rabih Kalakeche,* Takashi Hato,* Georges Rhodes,* Kenneth W. Dunn,*
Tarek M. El-Achkar,[†] Zoya Plotkin,* Ruben M. Sandoval,* and Pierre C. Dagher*

*Department of Medicine, Division of Nephrology, Indiana University, Indianapolis, Indiana; [†]Department of Medicine, Saint Louis University, and the Saint Louis Veterans Affairs Medical Center, Saint Louis, Missouri

ABSTRACT

Gram-negative sepsis carries high morbidity and mortality, especially when complicated by acute kidney injury (AKI). The mechanisms of AKI in sepsis remain poorly understood. Here we used intravital two-photon fluorescence microscopy to investigate the possibility of direct interactions between filtered endotoxin and tubular cells as a possible mechanism of AKI in sepsis. Using wild-type (WT), TLR4-knockout, and bone marrow chimeric mice, we found that endotoxin is readily filtered and internalized by S1 proximal tubules through local TLR4 receptors and through fluid-phase endocytosis. Only receptor-mediated interactions between endotoxin and S1 caused oxidative stress in neighboring S2 tubules. Despite significant endotoxin uptake, S1 segments showed no oxidative stress, possibly as a result of the upregulation of cytoprotective heme oxygenase-1 and sirtuin-1 (SIRT1). Conversely, S2 segments did not upregulate SIRT1 and exhibited severe structural and functional peroxisomal damage. Taken together, these data suggest that the S1 segment acts as a sensor of filtered endotoxin, which it takes up. Although this may limit the amount of endotoxin in the systemic circulation and the kidney, it results in severe secondary damage to the neighboring S2 segments.

Systemic Gram-negative sepsis remains the most challenging clinical condition encountered in hospitalized patients.[1] Despite increased awareness and early recognition, it often progresses rapidly and culminates in hemodynamic collapse and multiorgan failure. Vigorous therapeutic and supportive interventions, such as fluid resuscitation, pressors, and antimicrobials, have significantly improved the outcome of the septic patient.[2] Nevertheless, the overall morbidity and mortality from systemic sepsis, as well as the financial burden it generates, remain unacceptably elevated.[3]

The sepsis syndrome begins when Gram-negative bacteria find their way into the bloodstream. Endotoxin (lipopolysaccharide), both in its structural location in the outer membrane of the bacterial cell wall and as a freely shed molecule, interacts with cells of the innate immune system. This inter-

action is mediated primarily by TLR4, the endotoxin receptor and a member of the Toll-like receptor family of innate immune sensors.[4] Stimulation of TLR4 by endotoxin generates signaling that culminates in the production of a myriad of cytokines, like TNFα and IL-6, aimed at containing the infection.[5] These proinflammatory cytokines ultimately lead to the destruction of invading bacteria but can also cause collateral damage in tissues and organs. Indeed, the sepsis syndrome often progresses to cy-

tokine-mediated endothelial damage, vascular leak, hemodynamic collapse, and coagulation abnormalities.[6,7] End organ damage such as liver failure, myocardial depression, and AKI are thought to be secondary to perfusion defects as well as direct cytokine-mediated toxicity.

Acute kidney injury remains among the most dreaded complications of sepsis.[8,9] When it occurs, AKI negatively impacts the management of the septic patient by posing serious limitations to the choice of antimicrobial and fluid therapy, and by generating electrolyte abnormalities and uremic toxins that negatively impact the septic state. The pathology of the kidney examined in various animal sepsis models ranges from very subtle abnormalities to gross injury in the form of tubular and endothelial apoptosis, necrosis, vascular leak, and severe oxidative stress.[10–12] The reduction in GFR is traditionally ascribed to renal perfusion defects as well as the cytokine-mediated cellular damage to the endothelium and tubules.[13] Historically, interventions that are effective in treating animal models of sepsis-induced AKI have rarely met with success in the clinical arena. This is due in part to nonrepresentative animal models, inadequate clinical trials, and highly heterogeneous and complex patient population.[14,15]

We and others have documented the presence of TLR4 on renal tubular cells.[16,17] The presumed ability of TLR4 to sense endogenous "danger" ligands other than endotoxin has implicated this receptor in the pathophysiology of various forms of AKI, like ischemia-reperfusion, nephrotoxic injury, and local urinary tract infections.[18–20] A role for renal TLR4 in systemic sepsis is not obvious *a priori*. For such a role to exist, endotoxin in the blood stream has to find its way into the kidney and interact with locally expressed TLR4 on renal epithelial or endothelial cells. Indeed, we have recently shown, in a cecal ligation and puncture (CLP) model of sepsis in the rat, that endotoxin is readily filtered and taken up by proximal tubular cells.[13,17] Because endotoxin is not well retained after tissue fixation, intra vital 2-photon microscopy was essential in proving the accessibility of systemic endotoxin to renal tubular cells.

In this paper, we examine, in detail, the mechanism and outcome of direct interactions between systemically administered endotoxin and renal tubular cells. Using various strains of WT and KO mice, as well as bone marrow chimera mice, we implicate local renal TLR4 and CD14 in mediating signaling and uptake of endotoxin specifically by S1 segments of the proximal tubules. Using novel methodologies in live imaging, we show that interactions be-

tween endotoxin and S1 result in severe oxidative damage in neighboring S2 segments, independent from systemic cytokines. The molecules involved in the response of S1 to endotoxin, as well as the cross talk between S1 and S2, are examined in detail. Our studies establish, for the first time, the S1 segment as a primary sensor of endotoxin in the glomerular filtrate and uncover a new mechanism of direct renal damage by endotoxin in systemic sepsis.

RESULTS

Identification of S1 and S2 Proximal Tubular Segments

Two-photon live imaging of the mouse kidney cortex reveals two types of proximal tubules; one has very bright green punctuate autofluorescence near the apical portion of the cytoplasm. This likely represents pigments in apical endosomes and lysosomes. The second type of proximal tubules has less-intense green autofluorescence at the apical side (Figure 1A). Glomeruli and S3 segments of mice are located at depths beyond the reach of 2-photon microscopy. Using FITC-labeled inulin injected systemically, we show, in Figure 1B, that inulin always appears first in the lumen of tubules with low autofluorescence thus
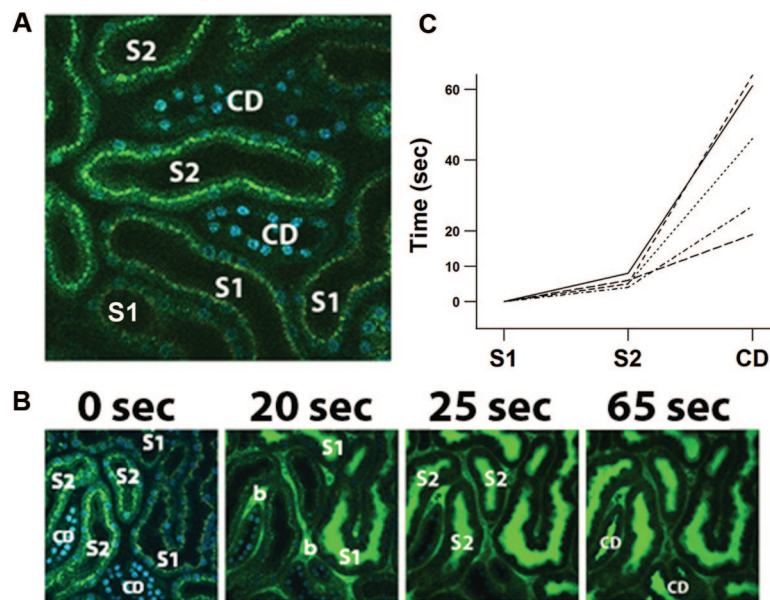
Figure 1. Identification of various renal cortical tubular segments. Live 2-photon microscopy of the mouse kidney reveals two types of proximal tubules that differ in the intensity of cellular green autofluorescence (A). The identity of the tubules was determined by detecting the time of appearance of FITC-labeled inulin in the tubular lumen (B). Inulin invariably appeared first in the lumen of tubules with low autofluorescence establishing their S1 identity. The appearance of inulin in S1 was nearly simultaneous with its appearance in peritubular capillaries (b). Inulin appeared on average 5 s later in the lumen of tubules with high autofluorescence (S2). The results of five such experiments are shown in (C). The appearance of inulin in distal segments and collecting ducts (CD), recognized by their lack of autofluorescence and intense blue Hoechst nuclear staining, was more variable. This is because distal tubules or CDs do not necessarily belong to the same nephrons as the proximal tubules present in the same field. Identical results were obtained in all mice strains.

establishing their upstream location. On average, inulin appears five seconds later in tubules with high autofluorescence, indicating their downstream location (Figure 1C and supplemental video 1). Because S3 segments in the outer stripe are not accessible to the 2-photon laser, we operationally define the tubules with low and high autofluorescence as S1 and S2, respectively. This operational definition, while not based on traditional anatomic or histologic parameters, is further supported by Supplemental Figure 1, which shows endotoxin uptake in S1 segments emerging from glomeruli. Indeed, we show below that endotoxin uptake is most prominent in tubules with low autofluorescence, thus confirming their S1 identity. The fluorescence signatures of S1 and S2 are best appreciated at 60x magnification and are common to all mouse strains used in the following studies.

## TLR4 Mediates Internalization of Endotoxin

We first conducted studies to determine whether endotoxin uptake was mediated by TLR4. To this end, we used a low endotoxin dose of 1 mg/Kg to distinguish receptor-mediated uptake from the robust fluid-phase endocytosis known to occur in proximal tubules. As shown in Figure 2A, WT mice exhibited significant uptake as early as 10 min after systemic endotoxin administration. By 90 min, the uptake increased significantly and had a patchy distribution among proximal tubules. High magnification views localized endotoxin uptake specifically to the apical regions of S1 proximal tubules of WT mice (Figure 1B). The S1 localization of endotoxin was further confirmed after euthanasia by examining kidney slices without fixation. Endotoxin was invariably seen in S1 segments near their glomerular origin (Supplemental Figure 1). With this dose of endotoxin, no uptake was observed in S2 segments. Similarly, TLR4 KO mice showed only minimal uptake at all time points indicating the dependence of this pathway on TLR4 receptors.

Preexposure to Endotoxin Enhances Endotoxin Uptake in S1 Segments of WT Mice

To further examine the question of TLR4-mediated endotoxin uptake, we took advantage of the fact that low-grade sepsis upregulates TLR4 expression in proximal tubules.[17] Thus, if endotoxin is internalized via TLR4, we would expect increased uptake of endotoxin in animals previously exposed to endotoxin. We therefore examined endotoxin uptake in animals preexposed to 0.25 mg/Kg unlabeled endotoxin 24 h before imaging. In WT mice, preexposure to endotoxin significantly increased fluorescence endotoxin uptake, which now peaked as early as 5 min after systemic administration (Figure 3A, 3B). The increase in endotoxin uptake was again localized to the S1 segment and was not observed in S2 segments. Similarly, preexposure to endotoxin did not affect endotoxin uptake in TLR4 KO mice, which remained minimal throughout (Figure 3C, 3D). Quantitation of endotoxin uptake for all groups is shown in Figure 3E.

Proximal Tubular Uptake of High-Dose Endotoxin in WT and TLR4 KO Mice

We next compared the uptake of high-dose endotoxin (5
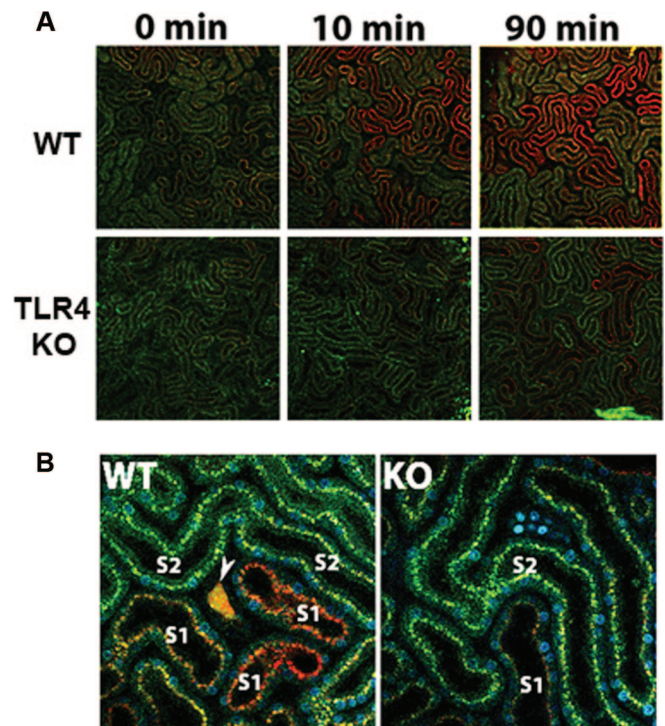
Figure 2. Proximal tubular uptake of low dose endotoxin in WT and TLR4 KO mice. Alexa 568-labeled endotoxin (red color) was injected systemically (1 mg/Kg) and its appearance in the kidney detected with live 2-photon microscopy. Green represents tubular autofluorescence. Nuclei are stained blue with Hoechst. Panel **A** shows 20x views of endotoxin uptake in WT and TLR4 KO mice over a period of 90 min. 60x views are shown in **B** at the 90-min time point for both mice strains and reveal that endotoxin uptake in WT mice is localized to S1 tubules. S2 tubules of WT and all tubules of KO showed minimal endotoxin uptake. Arrowhead points to concentrated endotoxin in a distal segment or collecting duct. Images are representative of n = 4 per group.

mg/kg) between WT and TLR4 KO mice. This commonly used dose in toxicity studies likely exceeds the saturation point of the receptor-mediated pathway and thus could uncover additional modes of endotoxin uptake. In WT mice, endotoxin was again observed to concentrate in S1 tubules with a coarse granular pattern. S2 tubules also exhibited endotoxin uptake, but this was significantly less intense and had a fine granular appearance (Figure 4). Both S1 and S2 segments showed slight collapse of the tubular lumen, possibly secondary to endotoxin-induced reduction in glomerular filtration. TLR4 KO mice showed only one pattern of endotoxin uptake in all tubules that was fine granular in appearance, similar to the one in S2 segments of WT mice. All tubules in TLR4 KO mice had normal morphology and widely patent lumens, indicating lack of any toxic effects of endotoxin. These data show that high-dose endotoxin can be taken up by proximal tubules via two routes: one that is TLR4-mediated and specific to S1 of WT mice and another that is shared by all tubules and likely represents fluid-phase endocytosis.
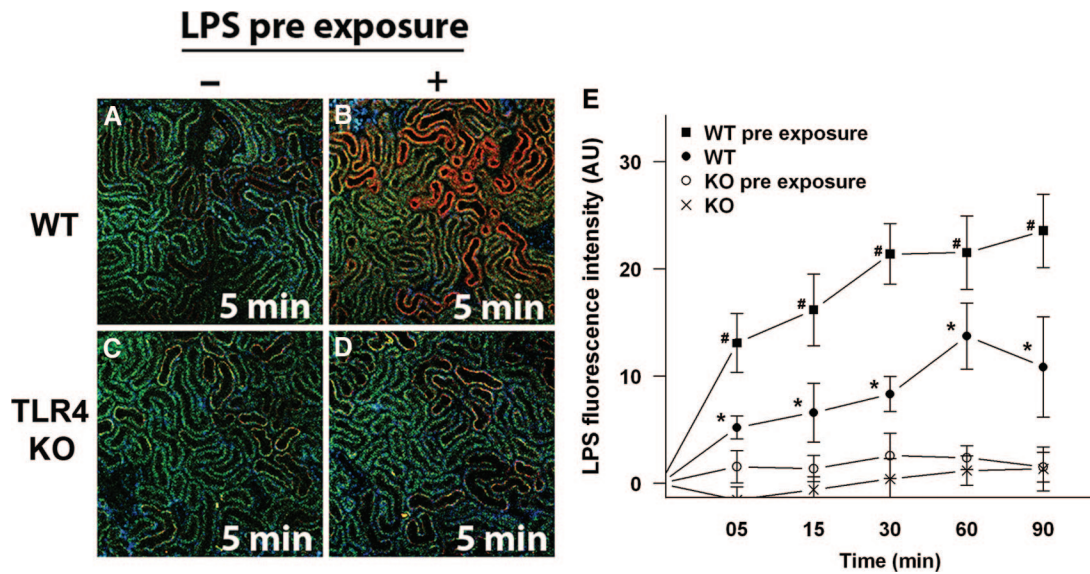
Figure 3. Preexposure to endotoxin enhances endotoxin uptake in S1 segments of WT mice. WT and TLR4 KO mice were pre exposed to vehicle or 0.25 mg/Kg unlabeled endotoxin 24 h before live 2-photon imaging. At the time of imaging, 1 mg/Kg Alexa 568-labeled endotoxin (red) was injected systemically. Preexposure to endotoxin caused enhanced uptake in S1 tubules of WT (**B**) but not KO mice (**D**), as early as 5 min after injection. Quantitation of endotoxin uptake in S1 tubules is shown at various time points for WT and KO mice, with and without preexposure to endotoxin (**E**, data are means ± SD and represent the average S1 tubular fluorescence per field. At least 20 fields were examined per mouse kidney, n = 3 mice per group. #$P<0.01$ compared to WT and both KO groups, *$P < 0.01$ compared to both KO groups).

TLR4-Mediated Uptake and Fluid-Phase Endocytosis Result in Differential Intracellular Sorting of Internalized Endotoxin

The intracellular effects and ultimate fate of internalized endotoxin depend, in part, on its sorting pathways. We therefore investigated whether TLR4-mediated uptake and fluid-phase endocytosis resulted in differential sorting of internalized endotoxin. To this end, we colocalized endotoxin with fluorescence low MW dextran, a marker of fluid-phase endocytosis. Low MW dextran was given 16 h before endotoxin and was thus allowed to reach its final lysosomal compartment. In WT mice, S1 segments showed clear evidence of dual sorting involving a TLR4-mediated pathway as well as fluid-phase endocytosis (Figure 5). This was best seen in animals preexposed to endotoxin because they exhibited significant TLR4-mediated endotoxin uptake that did not colocalize with low MW dextran (Figure 5C). The S2 segments in WT mice exhibited only fluid-phase endotoxin uptake that colocalized strongly with low MW dextran. Similarly, endotoxin uptake in TLR4 KO mice strongly colocalized with low MW dextran in all tubule segments. The visual appearance of a two-compartment model for endotoxin sorting in WT mice S1, as opposed to a one compartment model for WT S2 and KO tubules, is supported by a quantitative analysis of pixel red (endotoxin) and blue (low MW dextran) fluorescence intensities (Figure 5D and 5H).

Endotoxin-Induced Oxidative Stress Occurs Predominantly in S2 Segments of WT Mice

Widespread tissue oxidative stress is a prominent feature of sepsis. We therefore determined the segmental distribution of
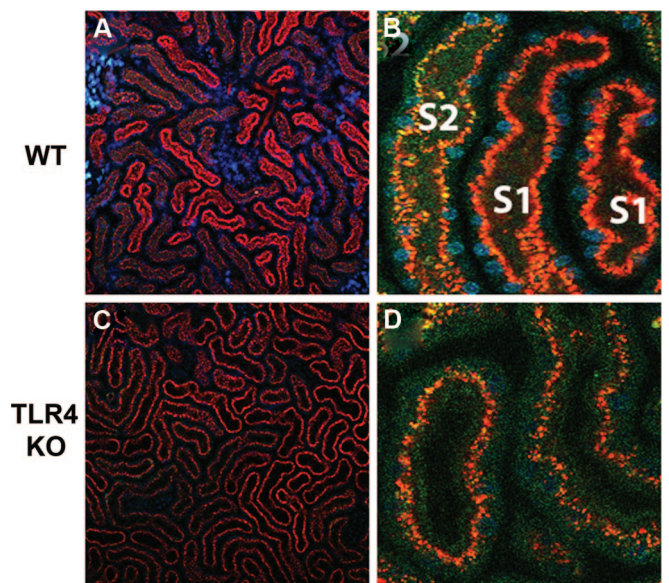
Figure 4. Proximal tubular uptake of high-dose endotoxin in WT and TLR4 KO mice. Alexa 568-labeled endotoxin (red, 5 mg/Kg) was injected systemically 4 h before 2-photon live imaging of the kidney. 20x views of the WT kidney (**A**) reveals markedly heterogeneous endotoxin uptake and tubular collapse as opposed to KO mice which showed more homogeneous uptake and normal tubular morphology (**C**). 60x views localize coarse granular uptake of endotoxin to S1 tubules of WT mice (**B**). S2 tubules of WT mice (recognized by their high autofluorescence in the green channel) and all tubules of TLR4 KO mice (**D**) showed less-intense endotoxin uptake that had a fine granular appearance.
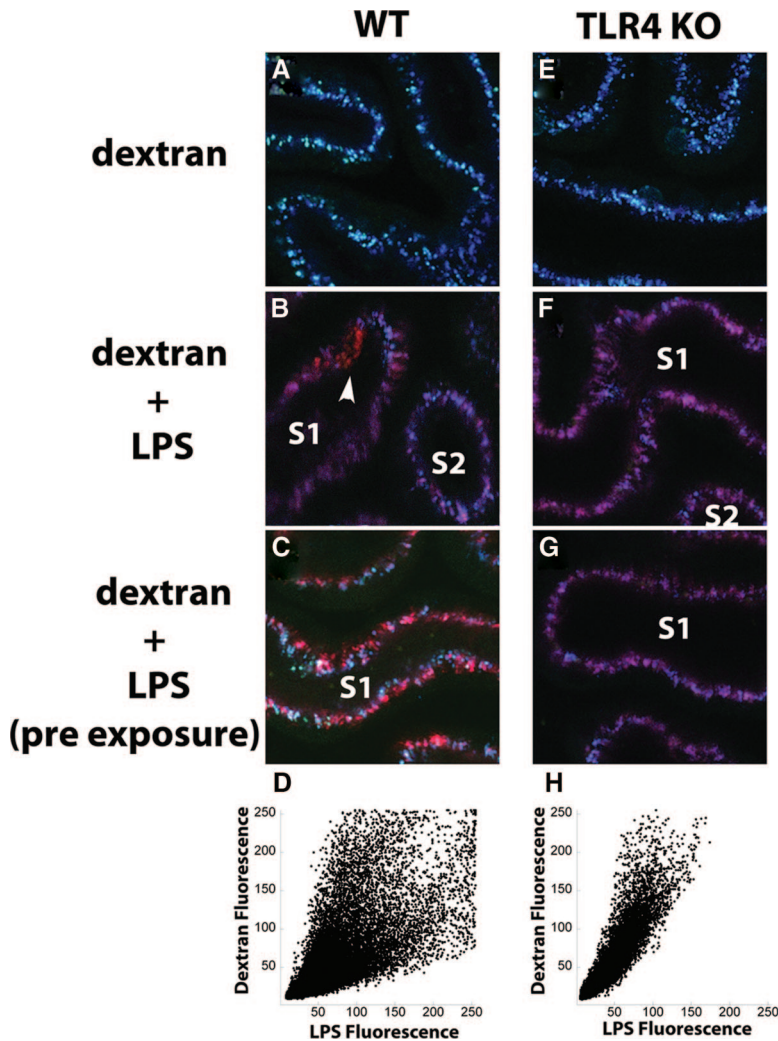
Figure 5. TLR4-mediated uptake and fluid-phase endocytosis result in differential intracellular sorting of internalized endotoxin. Cascade blue 4 KDa dextran, a marker of fluid-phase endocytosis, was injected systemically 16 h before imaging (**A**, **E**). Four hours before imaging, Alexa 568-labeled endotoxin 3 mg/Kg was injected systemically (**B**, **F**). Arrowhead in **B** points to red endotoxin that does not co localize with blue dextran in a S1 segment of WT mouse. S2 of WT and all tubules of TLR4 KO showed purple color indicating colocalization of red endotoxin with blue dextran. TLR4-mediated uptake of endotoxin in S1 of WT (but not KO) mice is even more evident when TLR4 receptors are upregulated with preexposure to 0.25 mg/Kg unlabeled endotoxin (**C**, **G**). Panels **D** and **H** show the distribution of red and blue fluorescence in each pixel from panels **C** and **G**, respectively. A two-compartment model is evident in WT but not TLR4 KO mice.

cellular and hemodynamic effects. To exclude such effects, we show, in Supplemental Figure 2A, that oxidative stress occurs in S2 but not S1, even when carboxy-DCFDA is administered before endotoxin. Furthermore, the low but measurable fluorescence of unoxidized carboxy-DCFDA allowed us to gauge the adequacy of S1 probe loading in the presence and absence of endotoxin (Supplemental Figures 2B and 2C). In TLR4 KO mice, which exhibit only fluid-phase endotoxin uptake, no oxidative stress was observed. Thus, the oxidative stress seen in S2 segments of WT mice is not secondary to the fluid-phase uptake of endotoxin in these tubules.

A major controversy exists as to the relative roles of renal parenchymal *versus* hematopoietic TLR4 in sepsis-induced oxidative stress and AKI. To address this question, we generated bone marrow chimera mice between WT and TLR4 KO strains and examined their response to endotoxin. As shown in Figures 6G and 6H, the presence of renal TLR4 (KO/WT) was essential for oxidative stress to occur. The oxidative stress noted in KO/WT chimeras localized primarily to S2 segments, as it did in total WT mice. Chimeras with TLR4 present only on peripheral leukocytes, but not the kidney (WT/KO), exhibited minimal oxidative stress comparable to that seen in total KO mice. These results suggest that oxidative stress in S2 segments is secondary to a local interaction between endotoxin and S1 tubules rather than systemic cytokines generated by endotoxin interacting with peripheral leukocytes.

To confirm these results and exclude possible artifacts specific to DCFDA, we used DHE, an oxidative stress probe with markedly different chemical and fluorescence properties (Figure 7). Identical results were obtained in all mice groups.

oxidative stress in relation to endotoxin uptake. In WT mice, endotoxin resulted in significant renal oxidative stress, as determined by carboxy-DCFDA fluorescence. Surprisingly, oxidative stress was localized specifically to S2 tubules (Figure 6). It was most prominent at the brush border early on but was fully cytoplasmic at later time points. In contrast, S1 tubules showed minimal oxidative stress despite their extensive endotoxin uptake. However, differences in carboxy-DCFDA fluorescence are also a function of its delivery and loading into cells, both of which can be influenced by endotoxin through its

These data indicate that the oxidative stress seen in S2 was secondary to TLR4-mediated interaction of endotoxin with S1 and was not an effect of systemic cytokines. The data also confirm the lack of oxidative stress in S1 tubules despite their extensive endotoxin uptake.

CD14 Is Involved in Endotoxin Uptake and Is Essential for the Induction of Oxidative Stress Signaling

CD14 is known to be involved in endotoxin-TLR4-MD2 interactions by being part of the large receptor complex that senses
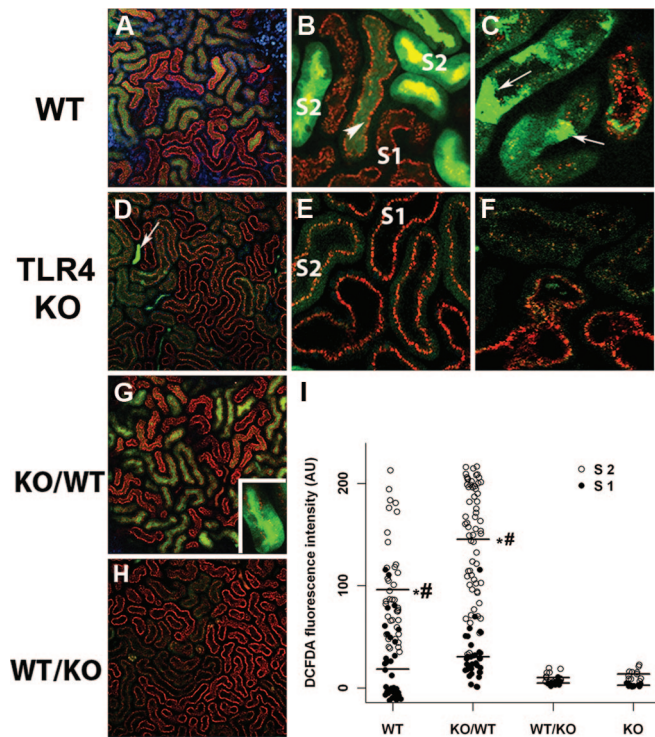
Figure 6. Endotoxin-induced oxidative stress measured with carboxy-DCFDA occurs in S2 segments of WT mice. Animals were injected systemically with Alexa 568-labeled endotoxin (red) 5 mg/Kg, 4 h before live imaging. Twenty min before imaging, carboxy-DCFDA (green) was injected systemically. 20x views reveal heterogeneous distribution of oxidative stress among tubules (**A**). 60x views localize oxidative stress predominantly to S2 tubules which exhibit minimal endotoxin uptake (**B**, arrow head points to an intermediate segment between S1 and S2). Twelve hours after endotoxin injection, carboxy-DCFDA fluorescence is fully cellular in S2 (**C**, arrows). TLR4 KO mice showed minimal oxidative stress at all time points (**D**, **E**, and **F**). Arrow in **D** points to concentrated carboxy-DCFDA in distal segment or collecting duct. Chimera mice generated through bone marrow transfer from TLR4 KO into WT recipient (KO/WT) exhibited oxidative stress similar to WT mice (**G**, inset is 60x view of one S2 tubule). The reverse chimera with bone marrow from WT into TLR4 KO mice (WT/KO) showed minimal oxidative stress (**H**). Panel **I** shows a scatterplot of carboxy-DCFDA fluorescence in S1 and S2 tubules of all groups (n = 4 per group, each point represents average fluorescence per tubule with bars indicating means. *P<0.01 compared with S1 same group, #P<0.01 compared with WT/KO and KO).

lipopolysaccharide.[21,22] Its exact roles in endotoxin presentation, uptake, and signaling are still controversial, especially in the kidney. Live imaging shows that endotoxin uptake by S1 tubules is maximal only in WT mice, where both TLR4 and CD14 are present (Figure 8). In the absence of CD14, the rate and magnitude of endotoxin uptake were about half the values observed in TLR4 KO and WT mice. Similarly, colocalization with low MW dextran revealed a predominance of fluid-phase endocytosis but not a complete absence of

TLR4-mediated uptake. Surprisingly, exposure of CD14 KO mice to endotoxin resulted in minimal oxidative stress that was similar in magnitude to that measured in TLR4 KO mice. Therefore, TLR4-mediated endotoxin uptake shows only a partial dependence on CD14. However, TLR4 signaling pathways that lead to oxidative stress seem to have an absolute dependence on CD14.
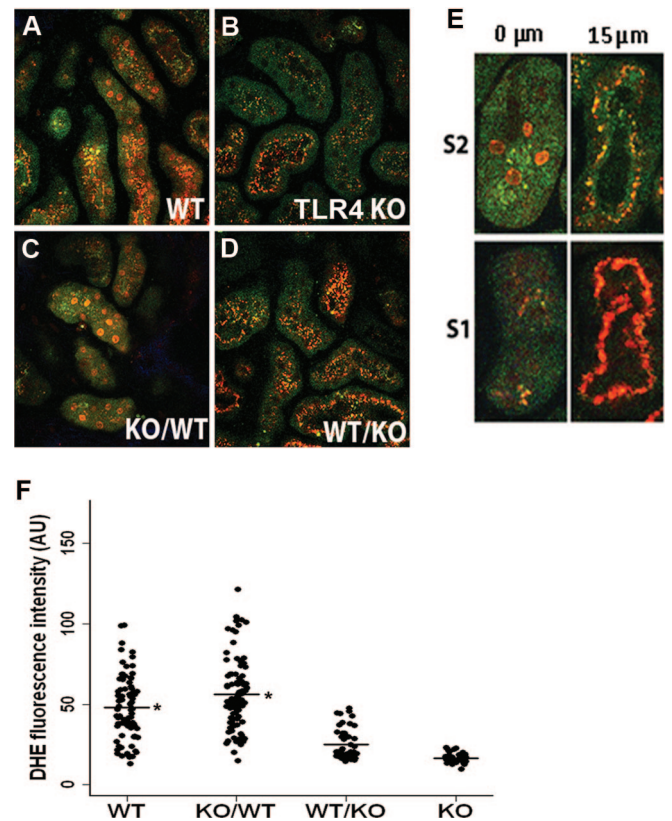
Figure 7. Endotoxin-induced oxidative stress measured with DHE occurs predominantly in S2 segments of WT mice. Animals were injected systemically with Alexa 568-labeled endotoxin (red, cytoplasmic) 5 mg/Kg 4 h before 2-photon live imaging. One hour before imaging, the oxidative stress probe DHE (nuclear red stain) was injected systemically. 20x views reveal oxidative stress (red orange nuclei) in some tubules of WT and KO/WT chimeras (**A**, **C**). KO mice and WT/KO chimeras showed no nuclear DHE fluorescence indicating lack of oxidative stress (**B**, **D**). Because imaging of nuclei done at the basal aspect of tubules does not allow full visualization of apical endotoxin, we took 60x planes at the basal (0 μm) and the apical (15 μm) aspects of tubules with and without nuclear DHE fluorescence (**E**). These show that tubules with strong nuclear DHE are indeed S2, with fine granular apical endotoxin uptake. S1 tubules with intense and coarse granular endotoxin uptake show no nuclear DHE staining (compare with Figure 4). Panel **F** shows a scatterplot of nuclear DHE fluorescence in all tubules of all groups (n = 4 animals per group. In each animal, at least 5 fields were examined. Each point represents total DHE fluorescence per nucleus with bars indicating means. *P < 0.01 compared with WT/KO and KO).
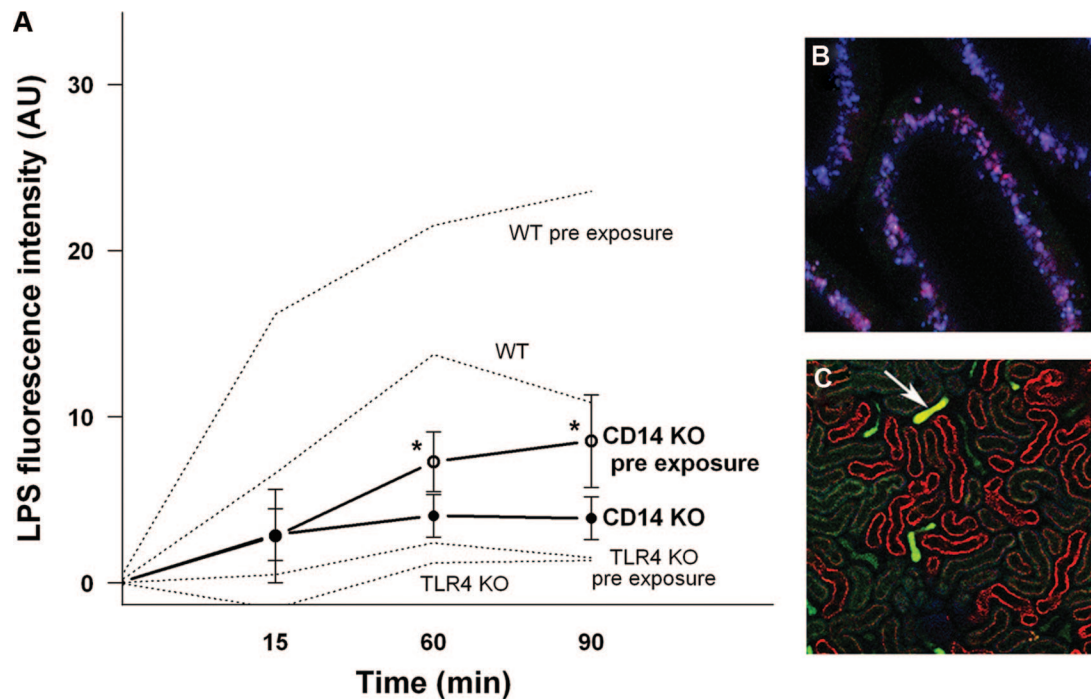
Figure 8. CD14 is involved in endotoxin uptake and is essential for the induction of oxidative signaling. In A, CD14 KO mice were injected with 1 mg/Kg Alexa 568-labeled endotoxin and imaged over 90 min. In the preexposure group, the animals were treated with 0.25 mg/Kg unlabeled endotoxin 16 h before imaging. Values represent means ± SD of LPS fluorescence intensity in S1 tubules. The graph of CD14 was superimposed on that of WT and TLR4 KO from Figure 3E. In **B**, endotoxin was co localized with cascade blue 3KDa dextran as described in Figure 5. In **C**, oxidative stress was measured with carboxy-DCFDA in CD14 KO, as described in Figure 6. Arrow in **C** points to concentrated carboxy-DCFDA in distal segment or collecting duct. (*$P < 0.05$ compared with CD14 KO).

## Molecules Involved in S1 Auto Protection and the Susceptibility of S2 to Oxidative Stress

The lack of oxidative stress in S1 tubules, despite their extensive endotoxin uptake, prompted us to examine the role of cytoprotective pathways that can oppose endotoxin-induced injury. Using immunofluorescence microscopy, we show, in Figure 9, that endotoxin uptake in S1 is accompanied by a robust expression of HO-1 and SIRT1, two cytoprotective molecules known to oppose oxidative stress.[23,24] In contrast, S2 tubules, while also up regulating HO-1 expression, failed to show any significant SIRT1 expression. We also examined peroxisomal integrity after endotoxin administration. Peroxisomes are prominent in S2 (and S3) segments and are involved in oxidative metabolic pathways.[25,26] In control mice, peroxisomes were clearly localized to S2 but were not observed in S1 segments. Endotoxin resulted in severe disruption of peroxisomes, as measured with structural (PMP70) and functional (catalase) markers.[27] Supplemental Figure 3 shows that oxidative stress in S2 was not accompanied by mitochondrial dysfunction, as measured by the membrane potential probe TMRM. This lends further support to the peroxisomal origin of the oxidative stress seen in S2.

Finally, we hypothesized that TLR4-mediated signaling in S1 generates cytokines such as TNFα, which, in turn, cause oxidative stress and peroxisomal damage in neighboring S2. While we did not succeed in staining for TNFα, we show, in

Figure 10, that TNFR1 expression in control kidneys is localized specifically to S2 but not S1 tubules. TNFR1 was also abundantly expressed on S3 segments (not shown). Endotoxin exposure resulted in decreased TNFR1 staining, suggesting intracellular degradation or shedding, both known to occur following activation of this receptor. These data provide indirect evidence for the susceptibility of S2 segments to the detrimental effects of TNFα and possibly other inflammatory cytokines.

DISCUSSION

In this paper, we applied 2-photon live microscopy to uncover a novel pathway of renal injury in a mouse model of systemic endotoxemia. While systemically administered endotoxin has been detected in the kidney before,[28,29] our studies provide the first high-resolution temporal and spatial imaging of interactions of this molecule with specific tubular segments as well as the outcome of such interactions. The results support a model in which endotoxin is readily filtered and interacts with S1 via locally expressed TLR4 receptors. This interaction causes S1 to secrete cytokines like TNFα, which result in oxidative stress in downstream S2 and S3 tubules. Interaction of endotoxin with local TLR4 on distal segments and collecting ducts has been shown by others and has relevance to the pathophysiology of lower urinary infection and pyelonephritis, where endotoxin
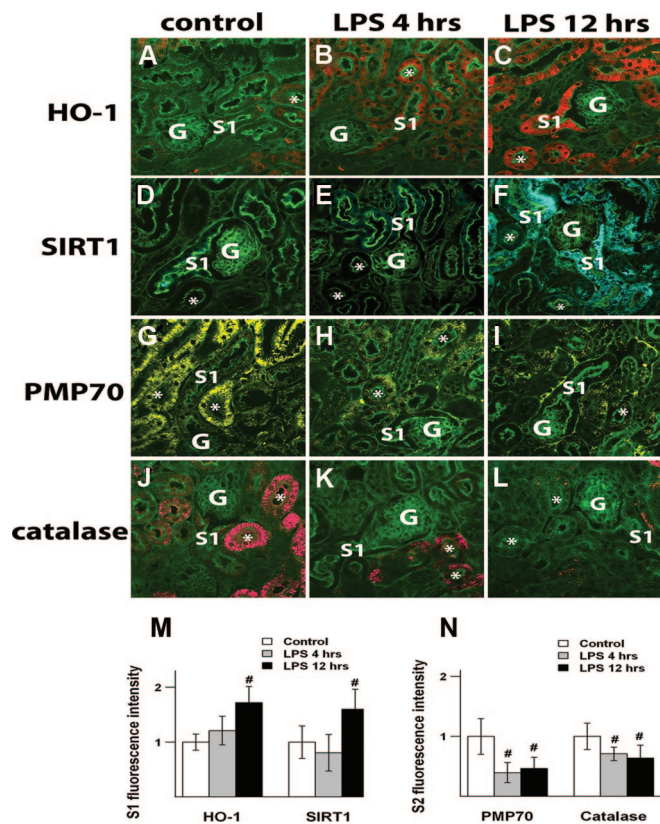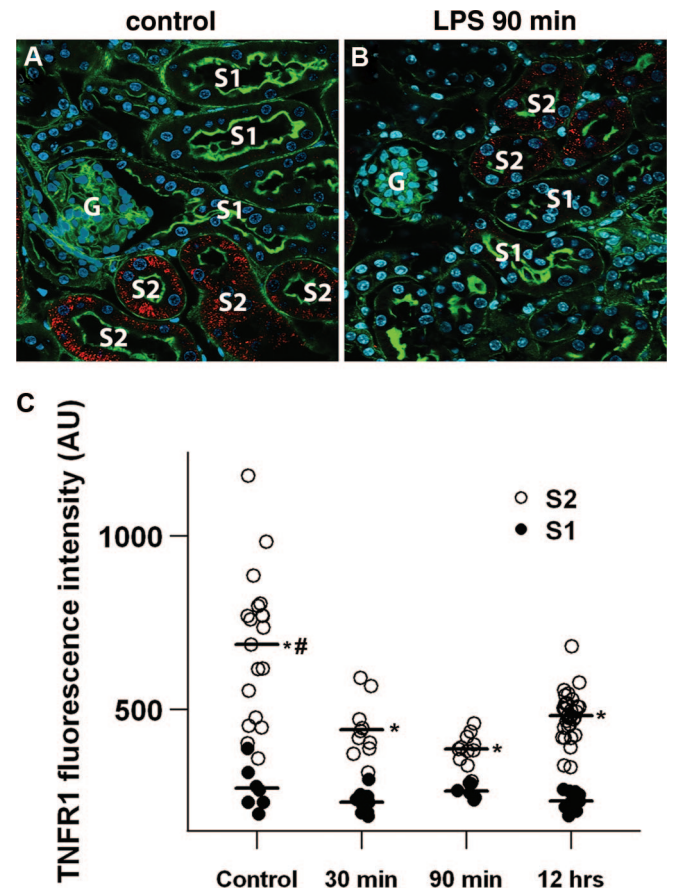
Figure 9. Effect of endotoxin on the expression of HO-1, SIRT1, and peroxisomal markers. Fixed kidney sections from WT mice were exposed to 5 mg/Kg unlabeled LPS and harvested at 4 or 12 h. Sections were stained for HO-1, SIRT1, PMP70, or catalase. After treatment with fluorescence secondary antibodies, they were imaged with a confocal microscope and pseudocolored for clarity. Green color is FITC-phalloidin staining of the apical brush border of proximal tubules. G denotes Glomeruli and * denotes S2, recognized by their thin brush border compared with S1. Fields shown are representative of at least 10 fields per section, taken from n = 3 animals per group. Panel **M** shows quantitation of fluorescence of HO-1 and SIRT1 in S1 tubules. Only S1 tubules seen to emanate directly from Bowman space were used for quantitation. Panel **N** shows fluorescence quantitation of PMP70 and catalase in S2 tubules. Values are means ± SD from n = 3 animals per group (#, $P < 0.01$ when compared with control group).

originates from within the urinary tract.[30–32] Our studies are the first to implicate endotoxin interaction with proximal tubules in the pathophysiology of systemic Gram-negative sepsis.

The lack of oxidative stress in S1 segments, despite their direct interaction with endotoxin, underscores their high potential for autoprotection. Such a phenomenon has been reported in monocytes after TLR4-mediated exposure to endotoxin.[33] Like monocytes, the S1 autoprotection mechanism seems to be dependent, in part, on upregulation of cytoprotective molecules with antioxidant properties. Indeed, HO-1 and the histone deacetylase SIRT1 have been reported to convey protection in various models of AKI.[23,24,34,35] In our model of

endotoxemia, the S1 segment acts as the "sensor" of endotoxin in the filtrate and, as such, autoprotects itself while simultaneously signaling to neighboring segments. This function of S1 segments is remarkably similar to that of Kupffer cells in the liver, which also signal the presence of endotoxin to neighboring hepatocytes.[36]

While S1 segments exhibit acute autoprotection from endotoxin signaling, they do uptake the molecule through a TLR4-mediated pathway. The ultimate outcome of this uptake is unknown and will require more prolonged imaging. We

Figure 10. Effect of endotoxin on TNFR1 expression in S2 tubules. Fixed kidney sections from control WT mice (**A**) and WT mice exposed to 5 mg/Kg unlabeled LPS and harvested 90 min later (**B**). Sections were stained with antibody for TNFR1 (red). Nuclei were stained blue with DAPI and green is FITC-phalloidin staining of apical brush border. G denotes glomeruli. S1 tubules are recognized by their thick brush border and occasionally are seen to emanate directly from Bowman space. S2 tubules have a thinner brush border compared with S1. Note the presence of TNFR1 staining in S2 tubules that decreases after endotoxin exposure. No TNFR1 staining is observed in S1. In **C**, a scatterplot of TNFR1 fluorescence intensity is shown in WT mice exposed to 5 mg/Kg endotoxin and harvested at various time points. (Values are average fluorescence intensity per tubule with the bars indicating the means, n = 3 mice per time point. *$P < 0.01$ compared with S1 at same time point. #$P < 0.01$ compared with S2 at 30 min, 90 min, and 12 h).

have previously localized TLR4 to the Golgi apparatus in fixed tissues.[17] Whether the Golgi apparatus is one of the destinations of internalized endotoxin remains to be determined.[37] The other pathway of endotoxin uptake in S1 is via fluid-phase endocytosis. An attractive possibility is that, through this pathway, S1 can act as a "sink" for the uptake and degradation of endotoxin. As such, it could convey systemic protection by eliminating circulating endotoxin. However, when faced with larger loads of this toxin, it is possible that this pathway can lead to cellular damage. Future studies will aim to investigate the long-term outcomes of endotoxin uptake on S1 segment function and viability.

Our studies with mouse chimeras are in apparent conflict with those of Cunningham *et al.*[38] In an elegant model of kidney cross-transplantation between TLR4 KO and WT mice, this group showed more injury when TLR4 was systemically present. However, they also clearly showed that renal TLR4 receptors alone are sufficient to cause renal injury in the presence of endotoxemia. In fact, the injury parameter used in these studies was blood urea levels. Urea levels, however, might not be reflective of intrinsic renal damage. Actually, urea levels are equally sensitive to prerenal states that can result from the hemodynamic effects of systemic cytokines. Our own results do not exclude an effect of systemic cytokines on GFR. Rather, our results specifically incriminate activation of TLR4 on S1 segments as the cause of more downstream oxidative stress.

The role of CD14 in endotoxin signaling and uptake remains very controversial.[39,40] The conflicting data are likely due to diverse functions and roles this molecule has in various cells and tissues. Our results indicate that endotoxin uptake has a partial dependence on CD14. It is possible that the presence or absence of CD14 directs endotoxin to different compartments and, ultimately, different cellular outcomes. Others have suggested that endotoxin uptake is separate from endotoxin signaling and might, in fact, be a signal termination event that can be mediated by CD14 alone.[39,41] Our data does not support such a model because TLR4 KO mice, presumably not deficient in CD14, showed essentially no receptor-mediated uptake. In contrast, TLR4-mediated signaling that resulted in oxidative stress was strongly dependent on CD14. Therefore, our data support a model in which CD14 can direct TLR4-signaling to specific signaling pathways with unique outcomes.[42,43]

The heterogeneity of tubular oxidative stress in endotoxemia models of sepsis is also seen in studies using video microscopy.[10] Our data with 2-photon microscopy offers superior resolution and localizes oxidative stress specifically to S2 tubules. While not directly observed in the live animal, *ex vivo* tissue examination shows that oxidative stress also extends to S3 segments. The S2 and S3 segments are metabolically distinct from S1 and share in common an abundance of oxidative pathways, some of which are localized to peroxisomes.[25] These organelles are, in fact, excellent markers of S2 (and S3) segments, as shown in our results. One aspect of their complex functions is to contain reactive species generated from oxidative pathways.[44] However, when injured, they become an actual source of oxidative damage to the cell. Indeed, our studies correlate S2 oxidative stress with severe peroxisomal injury, as determined with morphologic and functional markers.[45] Therefore, peroxisomes are both markers of, as well as players in, the severe S2 oxidative damage.

While others have documented the importance of TNFR1 in endotoxin-induced renal injury,[46] we have localized this receptor specifically to S2 and S3 tubules. This can explain the susceptibility of these segments to inflammatory cytokines. In fact, peroxisomal damage in other tissues has been shown to follow exposure to TNFα.[47] Furthermore, our studies point to an important role for locally produced TNFα by S1 in causing damage to S2. This is because WT/KO chimera mice, which can produce systemic TNFα in response to endotoxin, exhibited minimal renal oxidative stress. Thus, our data support a model in which S1 is the main source of TNFα acting on TNFR1 that is expressed on S2 and more downstream segments. This model also de-emphasizes the role of systemic TNFα produced by hematopoietic cells in causing direct renal injury. It does not, however, preclude reduced filtration related to systemic cytokine-induced hypotension. The final outcome of S2 and S3 cells following oxidative injury remains to be determined.

In conclusion, we have shown, for the first time, the specific mechanism and outcome of interactions between proximal tubules and filtered endotoxin. Live 2-photon microscopy was essential for the spatial and temporal resolution of these studies because of the poor retention of endotoxin after tissue fixation. The model that emerges from these data supports a role for S1 as the primary renal sensor of endotoxin in states of systemic Gram-negative sepsis. The receptor-mediated uptake of endotoxin by S1 tubules is dependent on locally expressed TLR4 and results in severe oxidative stress in tubular segments downstream of S1. This model can explain the occurrence of AKI in systemic sepsis even when hemodynamic parameters are well controlled. It also points to the processes of endotoxin filtration, S1 uptake and the cross talk between S1 and S2 segments as potential therapeutic targets.

CONCISE METHODS

Animals and Endotoxin

All animal protocols were approved by Indiana University Institutional Animal Care Committee and conform to the NIH Guide for the Care and Use of Laboratory Animals. Male mice strains C57BL/6J (background), B6.B10ScN-TLR4$^{lps-del}$/JthJ (TLR4 KO), and B6.129S-Cd14^{tm1Frm}/J (CD14 KO) were obtained from Jackson Labs. Mice were, on average, 8 to 12 wk old and weighed 20 to 30 g. Alexa 568 hydrazide (Invitrogen) was used to label endotoxin from *Salmonella Minnesota* (Re 595, Sigma) following established protocols.[48] The conjugate was separated from free probe using PD-10 columns (GE Healthcare Bio-Sciences). Biologic activity of the conjugate was determined through its ability to stimulate TNFα in cultured macro-

phages. All findings with our *Salmonella* endotoxin were replicated using Alexa 594-labeled endotoxin from E- coli (Invitrogen). *Escherichia coli* serotype 0128:B12 unlabeled endotoxin was also used in some experiments (Sigma). Low-dose endotoxin (1 mg/Kg) was given IV when imaging was performed immediately after administration. Large-dose endotoxin (5 mg/Kg) was given intraperitoneally 4 h before imaging.

Reagents

Oxidative stress was measured in the live mouse with two probes that differ in structure, membrane permeability, and pharmacokinetics. This was done to ensure that the cellular and tubular distribution of oxidative stress was not due in part to the intrinsic properties of one probe. First we used carboxy-2′, 7′-dichlorodihydrofluorescein diacetate (carboxy-DCFDA, Invitrogen), a sensor of overall cytoplasmic oxidative stress. The cell permeable probe has baseline green fluorescence in the unexcited state that can be used to gauge loading. Once exposed to reactive oxygen species, it emits bright green fluorescence. It was administered intravenously as a 7 mg/Kg bolus from a stock dissolved in ethanol and rediluted in normal saline. The second probe we used was dihydroethydium (DHE, Invitrogen), which detects specifically cytoplasmic superoxide. The unexcited probe has faint blue fluorescence. Once exposed to superoxide, it migrates to the nucleus where it binds DNA and emits bright red-orange fluorescence. It was injected intravenously as a 3 mg/Kg bolus from a DMSO stock rediluted in normal saline.

Tetramethylrhodamine methyl ester (TMRM, Invitrogen) was used to assess the mitochondrial membrane potential. It emits bright red fluorescence that is proportional to mitochondrial membrane potential. It was administered intravenously as a 10 μg/Kg bolus from a DMSO stock redissolved in normal saline. Cascade blue-labeled 3 KDa dextran (Invitrogen), a marker of fluid-phase endocytosis, was administered intraperitoneally as a 5 mg/Kg bolus around 16 h before imaging. This was done to allow dextran to undergo full endocytosis and label the fluid-phase endosomal compartment. Hoechst (nuclear stain, Invitrogen), dissolved in normal saline, was administed intraperitoneally as a 2 mg/Kg bolus 1 to 2 h before imaging. FITC-inulin (Sigma), a nonreabsorbable marker of tubular flow was obtained intravenously (25 ng/Kg).

Generation of Bone Marrow Chimeras

The procedure was performed at the Wells Cancer Center at Indiana University. In brief, Recipient mice are irradiated via a 139-Cs source with 1100 cGy total, given in two doses. Four days later, the mice were transplanted, via the lateral tail vein, with about 1 million bone marrow cells obtained from the long bones of donor mice. The degree of chimerism was assessed 8 wk later by flow cytometry using fluorescently labeled TLR4 antibodies. Alternatively, chimera were generated between TLR4 KO and Boy J background strains. Boy J mice are identical to C57Bl/6J except for the CD45.1 antigen, which is easier to detect by flow cytometry. Only animals where chimerism exceeded 95% were used.

2-photon Live Imaging of the Kidney

Live animal imaging was performed using a Bio-Rad MRC-1024MP Laser Scanning Confocal/Multiphoton scanner attached to a Nikon

Diaphot inverted microscope with a Nikon 20x or 60x NA 1.2 water-immersion objective.[49,50] Fluorescence excitation was provided by a Titanium-Sapphire laser (Spectraphysics, Mountain View, CA) 800 nm excitation and was used for all studies except TMRM, where 860 nm was used instead. Laser output was attenuated with neutral density filters to between 3% and 40% so that, after accounting for losses in the optical train of the microscope, we estimate that the power at the surface of the kidney was between 2 and 28 mw. Animals were placed on the stage with the exposed intact kidney placed in a cover-slip-bottomed cell culture dish (Warner Inst., Hamden, CT) bathed in isotonic saline, as we have described.[49] Quantitative analysis of acquired images was performed with Metamorph software.

Immunofluorescence Studies

Kidneys were perfused fixed *in situ* with 4% paraformaldehyde; 100 μm vibratome sections were permeabilized with 0.1% Triton X-100 and stained with primary antibodies for HO-1 (ab13243, Abcam), SIRT1(ab12193, Abcam), PMP70 (71–8300, Invitrogen), and catalase (ab1877, Abcam). TNFR1 stained best on 15 μm frozen section (ab19139, Abcam). Sections were counterstained with labeled secondary antibodies and imaged with a Zeiss confocal microscope, as described previously.[51,52]

Statistics

Data were analyzed for statistical significance with *R software*, using ANOVA and pairwise *t*-tests. Significance was set at $P < 0.05$.

DISCLOSURES
None.

REFERENCES

1. Mizushima N, Levine B, Cuervo AM, Klionsky DJ: Autophagy fights disease through cellular self-digestion. *Nature* 451: 1069–1075, 2008
2. Dellinger RP, Levy MM, Carlet JM, Bion J, Parker MM, Jaeschke R, Reinhart K, Angus DC, Brun-Buisson C, Beale R, Calandra T, Dhainaut JF, Gerlach H, Harvey M, Marini JJ, Marshall J, Ranieri M, Ramsay G, Sevransky J, Thompson BT, Townsend S, Vender JS, Zimmerman JL, Vincent JL: Surviving Sepsis Campaign: International guidelines for management of severe sepsis and septic shock: 2008. *Crit Care Med* 36: 296–327, 2008
3. Angus DC, Linde-Zwirble WT, Lidicker J, Clermont G, Carcillo J, Pinsky MR: Epidemiology of severe sepsis in the United States: Analysis of incidence, outcome, and associated costs of care. *Crit Care Med* 29: 1303–1310, 2001
4. Poltorak A, He X, Smirnova I, Liu MY, Van Huffel C, Du X, Birdwell D, Alejos E, Silva M, Galanos C, Freudenberg M, Ricciardi-Castagnoli P,

Layton B, Beutler B: Defective LPS signaling in C3H/HeJ and C57BL/10ScCr mice: Mutations in Tlr4 gene. *Science* 282: 2085–2088, 1998

5. Akira S: Toll-like receptor signaling. *J Biol Chem* 278: 38105–38108, 2003

6. Hotchkiss RS, Karl IE: The pathophysiology and treatment of sepsis. *N Engl J Med* 348: 138–150, 2003

7. Cohen J: The immunopathogenesis of sepsis. *Nature* 420: 885–891, 2002

8. Mehta RL, Kellum JA, Shah SV, Molitoris BA, Ronco C, Warnock DG, Levin A: Acute Kidney Injury Network: Report of an initiative to improve outcomes in acute kidney injury. *Crit Care* 11: R31, 2007

9. Uchino S, Kellum JA, Bellomo R, Doig GS, Morimatsu H, Morgera S, Schetz M, Tan I, Bouman C, Macedo E, Gibney N, Tolwani A, Ronco C: Acute renal failure in critically ill patients: A multinational, multicenter study. *JAMA* 294: 813–818, 2005

10. Wu L, Gokden N, Mayeux PR: Evidence for the role of reactive nitrogen species in polymicrobial sepsis-induced renal peritubular capillary dysfunction and tubular injury. *J Am Soc Nephrol* 18: 1807–1815, 2007

11. Dear JW, Yasuda H, Hu X, Hieny S, Yuen PS, Hewitt SM, Sher A, Star RA: Sepsis-induced organ failure is mediated by different pathways in the kidney and liver: Acute renal failure is dependent on MyD88 but not renal cell apoptosis. *Kidney Int* 69: 832–836, 2006

12. El-Achkar TM, Plotkin Z, Marcic B, Dagher PC: Sepsis induces an increase in thick ascending limb Cox-2 that is TLR4 dependent. *Am J Physiol Renal Physiol* 293: F1187–1196, 2007

13. El-Achkar TM, Hosein M, Dagher PC: Pathways of renal injury in systemic gram-negative sepsis. *Eur J Clin Invest* 38 Suppl 2: 39–44, 2008

14. Dyson A, Singer M: Animal models of sepsis: Why does preclinical efficacy fail to translate to the clinical setting? *Crit Care Med* 37: S30–S37, 2009

15. Rittirsch D, Hoesel LM, Ward PA: The disconnect between animal models of sepsis and human sepsis. *J Leukoc Biol* 81: 137–143, 2007

16. El-Achkar TM, Dagher PC: Renal Toll-like receptors: Recent advances and implications for disease. *Nat Clin Pract Nephrol* 2: 568–581, 2006

17. El-Achkar TM, Huang X, Plotkin Z, Sandoval RM, Rhodes GJ, Dagher PC: Sepsis induces changes in the expression and distribution of Toll-like receptor 4 in the rat kidney. *Am J Physiol Renal Physiol* 290: F1034–F1043, 2006

18. Wu H, Chen G, Wyburn KR, Yin J, Bertolino P, Eris JM, Alexander SI, Sharland AF, Chadban SJ: TLR4 activation mediates kidney ischemia/reperfusion injury. *J Clin Invest* 117: 2847–2859, 2007

19. Zhang B, Ramesh G, Uematsu S, Akira S, Reeves WB: TLR4 signaling mediates inflammation and tissue injury in nephrotoxicity. *J Am Soc Nephrol* 19: 923–932, 2008

20. El-Achkar TM, Wu XR, Rauchman M, McCracken R, Kiefer S, Dagher PC: Tamm-Horsfall protein protects the kidney from ischemic injury by decreasing inflammation and altering TLR4 expression. *Am J Physiol Renal Physiol* 295: F534–F544, 2008

21. Fearns C, Kravchenko VV, Ulevitch RJ, Loskutoff DJ: Murine CD14 gene expression in vivo: Extramyeloid synthesis and regulation by lipopolysaccharide. *J Exp Med* 181: 857–866, 1995

22. Akira S, Takeda K: Toll-like receptor signalling. *Nat Rev Immunol* 4: 499–511, 2004

23. Nath KA: Heme oxygenase-1: A provenance for cytoprotective pathways in the kidney and other tissues. *Kidney Int* 70: 432–443, 2006

24. Hasegawa K, Wakino S, Yoshioka K, Tatematsu S, Hara Y, Minakuchi H, Sueyasu K, Washida N, Tokuyama H, Tzukerman M, Skorecki K, Hayashi K, Itoh H: Kidney-specific overexpression of Sirt1 protects against acute kidney injury by retaining peroxisome function. *J Biol Chem* 285: 13045–13056, 2010

25. Usuda N, Yokota S, Hashimoto T, Nagata T: Immunocytochemical localization of D-amino acid oxidase in the central clear matrix of rat kidney peroxisomes. *J Histochem Cytochem* 34: 1709–1718, 1986

26. Schrader M, Fahimi HD: Peroxisomes and oxidative stress. *Biochim Biophys Acta* 1763: 1755–1766, 2006

27. Schrader M, Fahimi HD: The peroxisome: still a mysterious organelle. *Histochem Cell Biol* 129: 421–440, 2008

28. Musson RA, Morrison DC, Ulevitch RJ: Distribution of endotoxin (lipopolysaccharide) in the tissues of lipopolysaccharide-responsive and -unresponsive mice. *Infect Immun* 21: 448–457, 1978

29. Kang YH, Falk MC, Bentley TB, Lee CH: Distribution and role of lipopolysaccharide in the pathogenesis of acute renal proximal tubule injury. *Shock* 4: 441–449, 1995

30. Schilling JD, Martin SM, Hung CS, Lorenz RG, Hultgren SJ: Toll-like receptor 4 on stromal and hematopoietic cells mediates innate resistance to uropathogenic Escherichia coli. *Proc Natl Acad Sci U S A* 100: 4203–4208, 2003

31. Good DW, George T, Watts BA, 3rd: Lipopolysaccharide directly alters renal tubule transport through distinct TLR4-dependent pathways in basolateral and apical membranes. *Am J Physiol Renal Physiol* 297: F866–F874, 2009

32. Melican K, Boekel J, Mansson LE, Sandoval RM, Tanner GA, Kallskog O, Palm F, Molitoris BA, Richter-Dahlfors A: Bacterial infection-mediated mucosal signalling induces local renal ischaemia as a defence against sepsis. *Cell Microbiol* 10: 1987–1998, 2008

33. Rushworth SA, Chen XL, Mackman N, Ogborne RM, O'Connell MA: Lipopolysaccharide-induced heme oxygenase-1 expression in human monocytic cells is mediated via Nrf2 and protein kinase C. *J Immunol* 175: 4408–4415, 2005

34. Hasegawa K, Wakino S, Yoshioka K, Tatematsu S, Hara Y, Minakuchi H, Washida N, Tokuyama H, Hayashi K, Itoh H: Sirt1 protects against oxidative stress-induced renal tubular cell apoptosis by the bidirectional regulation of catalase expression. *Biochem Biophys Res Commun* 372: 51–56, 2008

35. He W, Wang Y, Zhang MZ, You L, Davis LS, Fan H, Yang HC, Fogo AB, Zent R, Harris RC, Breyer MD, Hao CM: Sirt1 activation protects the mouse renal medulla from oxidative injury. *J Clin Invest* 120: 1056–1068, 2010

36. Roberts RA, Ganey PE, Ju C, Kamendulis LM, Rusyn I, Klaunig JE: Role of the Kupffer cell in mediating hepatic toxicity and carcinogenesis. *Toxicol Sci* 96: 2–15, 2007

37. Latz E, Visintin A, Lien E, Fitzgerald KA, Monks BG, Kurt-Jones EA, Golenbock DT, Espevik T: Lipopolysaccharide rapidly traffics to and from the Golgi apparatus with the toll-like receptor 4-MD-2-CD14 complex in a process that is distinct from the initiation of signal transduction. *J Biol Chem* 277: 47834–47843, 2002

38. Cunningham PN, Wang Y, Guo R, He G, Quigg RJ: Role of Toll-like receptor 4 in endotoxin-induced acute renal failure. *J Immunol* 172: 2629–2635, 2004

39. Dunzendorfer S, Lee HK, Soldau K, Tobias PS: TLR4 is the signaling but not the lipopolysaccharide uptake receptor. *J Immunol* 173: 1166–1170, 2004

40. Jeyaseelan S, Chu HW, Young SK, Freeman MW, Worthen GS: Distinct roles of pattern recognition receptors CD14 and Toll-like receptor 4 in acute lung injury. *Infect Immun* 73: 1754–1763, 2005

41. Husebye H, Halaas O, Stenmark H, Tunheim G, Sandanger O, Bogen B, Brech A, Latz E, Espevik T: Endocytic pathways regulate Toll-like receptor 4 signaling and link innate and adaptive immunity. *EMBO J* 25: 683–692, 2006

42. Jiang Z, Georgel P, Du X, Shamel L, Sovath S, Mudd S, Huber M, Kalis C, Keck S, Galanos C, Freudenberg M, Beutler B: CD14 is required for MyD88-independent LPS signaling. *Nat Immunol* 6: 565–570, 2005

43. Gangloff SC, Zahringer U, Blondin C, Guenounou M, Silver J, Goyert SM: Influence of CD14 on ligand interactions between lipopolysaccharide and its receptor complex. *J Immunol* 175: 3940–3945, 2005

44. Bonekamp NA, Volkl A, Fahimi HD, Schrader M: Reactive oxygen species and peroxisomes: Struggling for balance. *Biofactors* 35: 346–355, 2009

45. Di Benedetto R, Denti MA, Salvati S, Attorri L, Di Biase A: PMP70

knock-down generates oxidative stress and pro-inflammatory cytokine production in C6 glial cells. *Neurochem Int* 54: 37–42, 2009

46. Cunningham PN, Dyanov HM, Park P, Wang J, Newell KA, Quigg RJ: Acute renal failure in endotoxemia is caused by TNF acting directly on TNF receptor-1 in kidney. *J Immunol* 168: 5817–5823, 2002

47. Contreras MA, Khan M, Smith BT, Cimini AM, Gilg AG, Orak J, Singh I, Singh AK: Endotoxin induces structure-function alterations of rat liver peroxisomes: Kupffer cells released factors as possible modulators. *Hepatology* 31: 446–455, 2000

48. Triantafilou K, Triantafilou M, Fernandez N: Lipopolysaccharide (LPS) labeled with Alexa 488 hydrazide as a novel probe for LPS binding studies. *Cytometry* 41: 316–320, 2000

49. Dunn KW, Sandoval RM, Kelly KJ, Dagher PC, Tanner GA, Atkinson SJ, Bacallao RL, Molitoris BA: Functional studies of the kidney of living animals using multicolor two-photon microscopy. *Am J Physiol Cell Physiol* 283: C905–C916, 2002

50. Kelly KJ, Sandoval RM, Dunn KW, Molitoris BA, Dagher PC: A novel method to determine specificity and sensitivity of the TUNEL reaction in the quantitation of apoptosis. *Am J Physiol Cell Physiol* 284: C1309–C1318, 2003

51. Kelly KJ, Plotkin Z, Vulgamott SL, Dagher PC: P53 mediates the apoptotic response to GTP depletion after renal ischemia-reperfusion: protective role of a p53 inhibitor. *J Am Soc Nephrol* 14: 128–138, 2003

52. Kelly KJ, Plotkin Z, Dagher PC: Guanosine supplementation reduces apoptosis and protects renal function in the setting of ischemic injury. *J Clin Invest* 108: 1291–1298, 2001

Supplemental information for this article is available online at http://www.jasn.org/.